Integrated Synthesis of Gold Nanoparticles Coated with Polyoxometalate Clusters

Sergio Martín,[a] Yohei Takashima,[a] Chang-Gen Lin,[b] Yu-Fei Song,[b] Haralampos N. Miras*[a] and Leroy Cronin*[a]

[a]School of Chemistry, University of Glasgow, Glasgow, G12 8QQ, U.K

[b]Beijing Advanced Innovation Center for Soft Matter Science and Engineering, State Key Laboratory of Chemical Resource Engineering, Beijing University of Chemical Technology, Beijing 100029, P. R. China

State Key Laboratory of Chemical Resource Engineering, Beijing University of Chemical Technology, Beijing 100029, P. R. China

Supporting Information Placeholder

ABSTRACT: Polyoxometalates (POMs) have been found to be good end-capping ligands for gold nanoparticles (AuNPs). Herein we introduce a new synthetic method to synthesize gold nanoparticle-POM hybrids by heating a solution of $AuNO_3(PMe_3)$ in acetonitrile in the presence of appropriate POM species with tetrabutyl-ammonium (TBA) as a counter-cation at 120 °C in a microwave. This method allowed us to produce POM-capped AuNPs without over reduction of the solution causing decomposition or reorganization of the POMs. Analysis of the resulting material by TEM showed that the POM's size, charge and functionality are key factors controlling the resulting POM-AuNP hybrid structure. Additionally, the reaction was monitored by ESI-MS, UV-Vis spectroscopy and DLS. The ESI-MS studies reveal crucial information regarding the nature of the reaction that takes place, showing the cation-exchange between Au(I) and tetrabutyl-ammonium (TBA) cations, followed by self-reduction of the Me3PAu(I)-POM complex.

INTRODUCTION

Polyoxometalates (POMs) are discrete negatively charged inorganic metal oxide clusters with fascinating properties and applications in diverse research areas ranging from catalysis to medicine and biology.[1–7] This is because POM clusters represent a large family of compounds which exhibit a wide range of shapes, sizes and topologies. Due to their polyanionic nature, structural diversity and redox properties, POMs also have been employed as end-capping ligands for nanoparticle synthesis.[8,9] Exploration of their redox activity led to the development of various synthetic methodologies for nanoparticle formation: (1) chemical reduction, the use of chemical reductants such as $NaBH_4$, H_2, ascorbic acid and Zn trigger the formation of POM nanoparticles;[10–15] (2) photochemical reduction, POMs can act as reducing agents as well as end-capping ligands upon photo-reduction by UV light irradiation[16–20] or gamma (γ) irradiation;[21] (3) electrochemical reduction, reduced POMs generated by bulk electrolysis and later used as reductants for the synthesis of nanoparticles;[22,23] (4) reduction by POMs with "built-in reducing ability", POMs with d-electron containing metal ions (ex. Mo^{V} or V^{IV}) have intrinsically reducing ability, enabling the nanoparticle synthesis in the absence of chemical additives and/or external stimuli.[24–26]

Alternatively, POM-capped nanoparticles can also be synthesized following a ligand exchange approach. For example, alkanethiol or citrate ligands can be exchanged successfully with a POM species.[27,28] The main advantage of this method is the employed mild reaction conditions, without utilization of complex routes and over reduction of the system which can be a problem for the stabilization of NPs by different POM structures. Weinstock and co-workers have achieved great success in developing rational synthetic approaches for the coating the surfaces of nanoparticles with POM ligands followed by detailed characterization with cryo-TEM.[29–31] Their method is robust with careful control of the pH and redox potential.

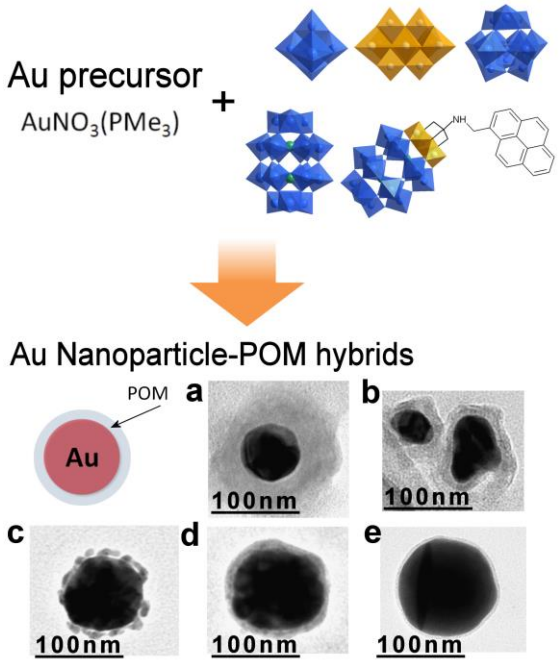

Figure 1 Schematic image of gold nanoparticle-POM hybrid using: a) W_6, b) V_{10}, c) W_{12}, d) W_{18} and e) $W_{15}V_3$-pyrene. The average size of the NP in the bottom three images is 100 nm in diameter.

Herein, we report a new synthetic method to form gold nanoparticle-POM hybrids (AuNP-POMs) without involving reduction of the POM species. The hybrids were easily synthesized upon heating both the gold and POM precursors. In addition, the resulting hybrids exhibited different levels of nanoparticle's surface coating depending on the size, charge and functionality of the POMs (Figure 1). The reaction was also monitored using electrospray ionization mass spectrometry

(ESI-MS), which has been proven to be a powerful tool for monitoring reactions and reveal reactivity details and formation of intermediate species. Additionally, ESI-MS can be used to identify the nature of the intermediates and compositions of coordination, organometallic and cluster compounds.[32–34] In this case, ESI-MS studies revealed some information regarding the first step of the reaction involving the cation exchange between $AuNO_3(PMe_3)$ and POMs and the thermally induced reduction of Au(I)-POM complexes. Finally, dynamic light scattering (DLS) provided was to monitor the growth of the gold nanoparticles.

RESULTS AND DISCUSSION

Synthesis of gold nanoparticles-POM hybrids. We selected $AuNO_3(PMe_3)$ as a metal precursor for formation of the AuNP hybrids since there is precedent for describing the observation that it can decompose to metallic Au after undergoing a thermally induced reduction process.[35] Indeed, in our experiments we found that a brown powder is obtained by heating $AuNO_3(PMe_3)$, which we determined to be metallic gold by powder X-ray diffraction (PXRD) measurements (Figure. 2a). The decomposition process in solution was also confirmed by ^{31}P.NMR (Figure 2b), showing the decrease of peak intensity associated with the precursor.

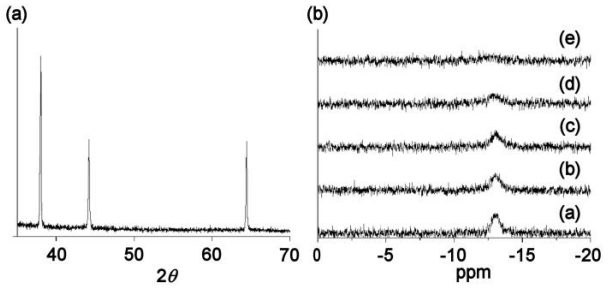

Figure 2 (a) PXRD patterns of gold metal synthesized by heating the CH_3CN solution with $AuNO_3(PMe_3)$ at 120 °C. The three peaks observed (2θ = 38.0°, 44.2° and 64.6°) correspond to the diffractions from the {1 1 1}, {2 0 0} and {2 2 0} planes of face-centered cubic of gold, respectively. (b) ^{31}PNMR spectra of $AuNO_3(PMe_3)$ in CD_3CN after heating at 85 °C for (a) 0 h, (b) 3 h, (c) 5 h, (d) 20 h and (e) 90 h.

The gold nanoparticle-POM hybrids were successfully synthesized upon microwave heating of a CH_3CN solution of $AuNO_3(PMe_3)$ in the presence of appropriate POM species at 120 °C. Although it appears that $AuNO_3(PMe_3)$ precursor is crucial, we did not attempt to elucidate the mechanism in this work, initially focusing on the phenomenological results demonstrating the integrated formation of AuNP-POM hybrids according to the following scheme:

$$Au(I)(NO_3)PMe_3 \xrightarrow[POM(TBA)_n]{\text{Microwave}} Au(0)NPs \text{ (scheme 1)}$$

The effect on the AuNP-POM hybrid formation utilizing six different POM species with different sizes, overall charge and functionalities has been explored using the following clusters: $((TBA)_2[W_6O_{19}]$; $\{W_6\}$, $(TBA)_3[H_3V_{10}O_{28}]$; $\{V_{10}\}$, $(TBA)_4[H_4W_{12}O_{40}]$; $\{W_{12}\}$, $(TBA)_6[P_2W_{18}O_{62}]$; $\{W_{18}\}$,$(TBA)_5H[P_2W_{15}V_3O_{62}(NC_{21}H_{18})]$; $\{P_2W_{15}V_3$-pyrene$\}$ and $(TBA)_{13}H_{23}K_4[P_8W_{48}O_{184}]$; $\{W_{48}\}$; TBA = tetrabutylammonium). It is worth noting that the POMs themselves do not appear to be reduced under the reaction conditions. Instead the microwave heating induces the decomposition of the $Au(NO_3)PMe_3$, during which the color of the solution turns purple. However, the UV-Vis spectra of the solution after completion of the reaction exhibited clear differences depending on the POM species, utilized see Figure 3. The extent of surface coverage by POM species affects the thickness of the POM layer as well as the average size distribution which is reflected to the observed shifts in the UV-vis maxima.

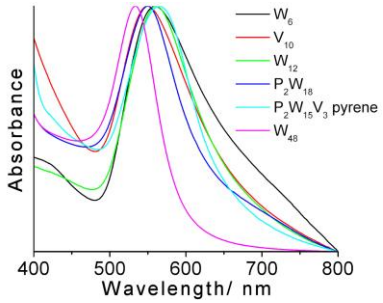

Figure 3 UV-Vis spectra of gold nanoparticles with various POMs.

In the case of $\{W_6\}$ and $\{V_{10}\}$, the gold nanoparticles were coated more effectively by POMs, even after the purification process, results in the stabilization of nanoparticles. When using POMs with higher negative charges, better coverage of the NP's surface was achieved. In the case of $\{W_{12}\}$ with four negative charges, they were attached on the surface of nanoparticle as small sized aggregates of approximately 5-7 nm. On the contrary, in the case of Dawson-type POMs $\{P_2W_{18}\}$ and $\{P_2W_{15}V_3$-pyrene$\}$, we observed a more homogeneous organization on the surface, with the $\{P_2W_{18}\}$ species exhibiting a slightly higher level of aggregation in comparison to the pyrene derivatized species. Finally, the use of the largest available cluster, $\{W_{48}\}$, with the highest negative charge, led to the formation of highly aggregated NPs. In this case electrostatic repulsions and steric hindrance prevented the POM clusters from effectively coating the NPs, see Figure 4.

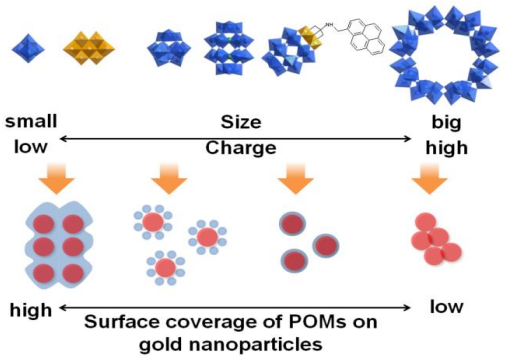

Figure 4 Conceptual representation of the observed nanoparticle-POM hybrids' surface coverage as a function of the POM's features.

The existence of POM-coated gold nanoparticles was confirmed by transmission electron microscopy (TEM), showing clear differences as a function of the POMs properties (Figure 5). Importantly, the reaction solutions were purified by dialysis treatment with CH_3CN/H_2O mixed solvent, prior to the TEM measurements; during this process (Figure 5), POMs

could show some level of organization both on, or around the gold nanoparticles, accompanied by the removal of excess POMs. In addition, Energy Filtered TEM (EFTEM) measurements were conducted to investigate the distribution of gold nanoparticles and POMs, showing that the gold nanoparticles were surrounded by POMs (Figure 6).

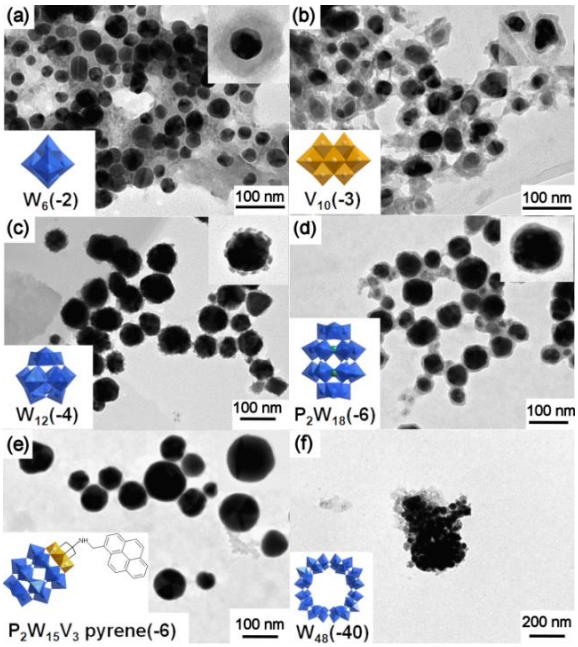

Figure 5 TEM images of gold nanoparticles with six kinds of POMs. Insets at the lower left: POMs and their charges used in the syntheses;{W_6}: $(TBA)_2[W_6O_{19}]$, {V_{10}}: $(TBA)_3[H_3V_{10}O_{28}]$, {W_{12}}: $(TBA)_4[H_4W_{12}O_{40}]$, {P_2W_{18}}: $(TBA)_6[P_2W_{18}O_{62}]$, {$P_2W_{15}V_3$pyrene}: $(TBA)_5H[P_2W_{15}V_3O_{62}(NC_{21}H_{18})]$, {$W_{48}$}: $(TBA)_{13}H_{23}K_4[P_8W_{48}O_{184}]$. Insets at the upper right: High magnification images.

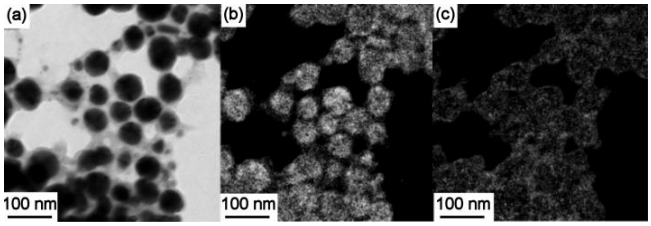

Figure 6 (a) Bright field TEM image of gold nanoparticle with {P_2W_{18}} and corresponding EFTEM images showing (b) Au and (c) W elements.

The differences observed in the hybrids formed depends greatly upon the size and charge of the POM species utilized (Figure 6). In the case of {W_6} and {V_{10}}, which are small in size and overall negative charge, they showed a tendency for easier aggregation even in the solution due to minimum steric and electrostatic repulsion. A lower coverage of {V_{10}} compared to {W_6} also supports this. This may be due to the fact that larger repulsion leads to smaller POM aggregates, resulting in a small domain for {W_{12}} and layer formation for {P_2W_{18}} and {$P_2W_{15}V_3$-pyrene}. The smaller POM coverage observed in the case of {$P_2W_{15}V_3$-pyrene} is also likely due to steric hindrance induced by the pyrene group leading to less aggregation. In contrast, almost all the {W_{48}} species were removed during the purification process, presumably due to a high degree of electrostatic repulsion. Additionally, the wheel shaped {W_{48}} appears to interact less well with the surface of the nanoparticles.

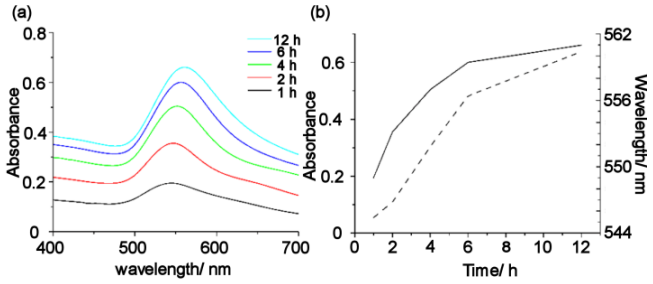

Figure 7 UV-vis data recorded during the gold nanoparticle synthesis in the presence of $(TBA)_4[H_4W_{12}O_{40}]$. (a) Selected UV-vis spectra showing the evolution of the surface plasmon resonance peak. (b) Intensity absorbance maxima and observed shift of the plasmon resonance peak in the spectrum as a function of time.

TEM studies on the reaction mixtures showed the inability of {W_{48}} species to interact efficiently with the gold nanoparticles. Instead, the AuNPs formed were spatially separated by the {W_{48}} species, resulting in narrower absorption band in UV-Vis spectrum (Figure 3). These results indicated that the aggregation of NPs depend upon the POMs size, charge and consequently the POMs ability for effective surface coverage.

Monitoring the reaction with UV-Vis and DLS. In an effort to investigate aspects of the reaction that leads to the formation for POM-NPs, we monitored the reaction by UV-Vis and DLS measurements in the case of {W_{12}}. The UV-Vis spectra showed a shift of the absorption band from 545 to 560 nm accompanied by an increase of the absorbance maximum (Figure 7a). Figure 7b shows the position and intensity of the plasmon resonance band as a function of the reaction time. The rapid increase of the absorbance up to 6 h indicates a fast formation of particles. As such, the dynamic light scattering (DLS) measurements allowed more direct information regarding the size and number of the nanoparticles. Figure 8 reveals an increase in particle size is accompanied by a small increase of the polydispersity of particles without changing the average number.

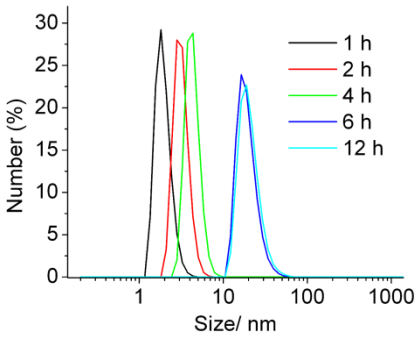

Figure 8 DLS data recorded during the gold nanoparticles synthesis in the presence of $(TBA)_4[H_4W_{12}O_{40}]$ after heating for 1, 2, 4, 6 and 12 h.

Moreover, between 4 and 6 h the particle size shows a sudden increase to 20 nm accompanied by a decrease of their population which is in agreement with the coalescence of the particles. The increase of particle concentration and the relatively weak coordination ability of POMs seems to be responsible for the coalescence. Finally, between 6 and 12 h revealed very small changes of the particle size, suggesting that most of the

$Au(NO_3)PMe_3$ has already been consumed in the early stages of the reaction.

Monitoring the reaction with ESI-MS. ESI-MS is a powerful tool for the precise determination of composition and speciation studies of reaction mixtures.[36–40] In order to investigate the reaction that leads to the formation of NP-POM hybrids in more detail, ESI-MS measurements were conducted before and after the reaction. The spectrum obtained from the mixture before the reaction, Figure 9a, clearly shows peaks which can be assigned to $(TBA)NO_3$ and $Au(NO_3)PMe_3$ respectively, indicating that the TBA cations associated with the POM species can easily undergo a cation exchange process with gold(I) cation even at ambient temperature. Additionally, it was possible to identify peaks associated to the complex formed between Au(I) and POM in the high *m/z* region (Figure 9b). It is worth noting that no reaction occurs in the case where $AuClPMe_3$ was used as gold precursor. This initial cation exchange step is key for the effective stabilization of nanoparticles by the POMs which will form upon the reduction of Au(I) source. The low *m/z* region of the spectrum recorded from the reaction mixture upon completion of the reaction (Figure 9c) showed a decrease of the peak associated to the $Au(NO_3)PMe_3$ which indicates the consumption of the Au(I) source during the nanoparticle formation and the appearance of new small peak which could be assigned to $Au(NO_3)(PMe_3)_2$. The appearance of $Au(NO_3)(PMe_3)_2$ suggests that unreacted traces of $Au(NO_3)PMe_3$ traps free PMe_3 groups produced from the decomposition process of $Au(NO_3)PMe_3$. The high *m/z* region of the spectrum provides additional evidence for the initial stages of the reaction (Figure 9d); most of the peaks initially associated to the complexes between $Au(NO_3)PMe_3$ and $\{W_{12}\}$ clusters appeared to have their intensity dramatically reduced after the reaction. On the other hand, the peaks assigned to the gold-POM complexes associated with one TBA (*m/z* = 1655-1700) and without TBA (*m/z* = 1529-1572) cations increased their intensity whilst the species associated with two TBA cations (*m/z* = 1800-1835) have been decreased, indicating that the cation exchange between TBA and gold cation plays a key role during the reaction.

The combination of data obtained from UV-Vis, DLS and ESI-MS revealed some important information in regard to the species involved in the reaction that takes place in this case and it is shown in Figure 10. The formation of nanoparticles observed at the early stages of the reaction, is associated with the decomposition of gold-POM complexes triggered by a cation exchange process between the $Au(NO_3)PMe_3$ and $\{W_{12}\}$ species followed by the rapid increase of their average size. The observed size increase of the nanoparticles is based on the coalescence of the nanoparticles as a function of the time (Figures S3-S5†). It has been reported that the existence of the Au(III) intermediate species is due to disproportionation,[41–43] however, we were not able to detect any Au(III) species during the ESI-MS studies, suggesting that Au(I) is directly reduced to Au(0). This is potentially important in terms of efficiency and prevention of potential side reactions which could affect the atom economy and/or the homogeneity of the hybrids generated.

CONCLUSIONS

In conclusion, we have introduced a new and easy synthetic method to prepare gold nanoparticle-POM hybrids. The presence of the POM species in solution is crucial for the prevention of uncontrolled and random aggregation of NPs. We have demonstrated that the POMs provide an elegant, energy efficient and facile way to initiate the reduction and subsequent controlled growth of Au-NPs. We also showed that smaller POMs such as $\{W_6\}$ and $\{V_{10}\}$ with smaller negative charges could easily coat and stabilize NPs due to their smaller steric and electronic repulsions, leading to more efficient coating of gold nanoparticles' surface with POM species. Additionally, larger POMs with a high negative charge demonstrated different interactions, which influences the surface's coating of gold nanoparticles. In the case of $\{W_{12}\}$ and $\{P_2W_{18}\}$ clusters form uniform POM layers on the surface while in the case of $\{W_{48}\}$ no distinct surface organization was observed.

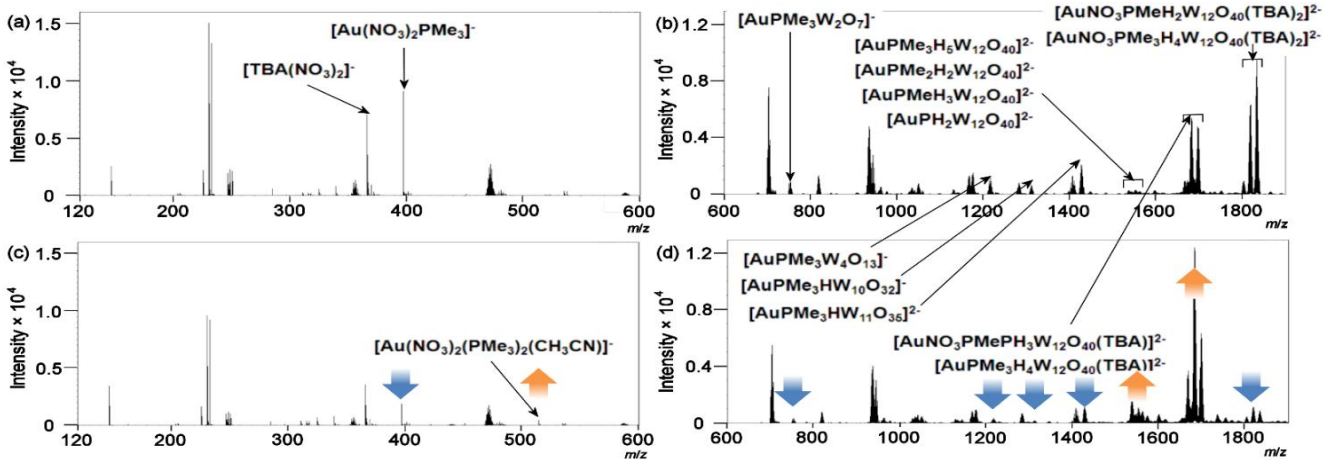

Figure 9 ESI-MS spectra of reaction mixture ($AuNO_3(PMe_3)$ + $(TBA)_4[H_4W_{12}O_{40}]$). (a) before reaction (m/z = 120 - 600) (b) before reaction (m/z = 600 – 1900) (c) after reaction (m/z = 120 – 600) (d) after reaction (m/z = 600 – 1900). Orange and blue arrows indicate increase and decrease of their peak intensities after reaction, respectively.

Finally, we demonstrated also that the ESI-MS spectroscopy can be useful to monitor the different species that form during the reaction of the starting materials and are crucial for the further development of NPs; the cation exchange between $AuNO_3(PMe_3)$ and POMs species has been proven to be a crucial step at the early stages of the reaction, and subsequent initiation of gold nanoparticles formation during the heat induced reduction. Moreover, UV-Vis absorption and DLS were used to monitor the direct conversion of gold precursor to gold nanoparticles followed by further rapid growth. Out observations are summarized in Figure 10.

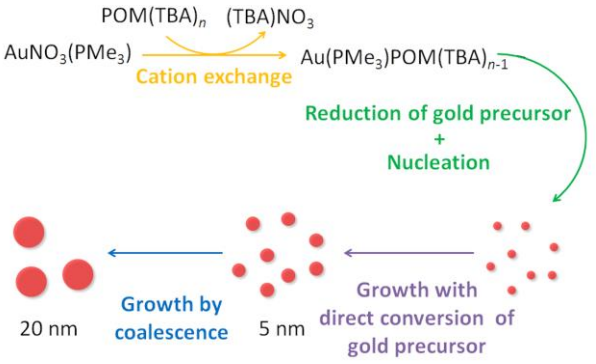

Figure 10 Schematic representation of the reaction steps leading to the formation of POM-NP hybrids.

A noteworthy advantage of this synthetic method is the fact that it is possible to form gold nanoparticle-POM hybrids without the use of additional internal (e.g. chemical reductants) or external stimuli (e.g. UV light irradiation). This is important since allows us to use any known POMs species with various topologies and charges, including those that are unstable to chemical or photo- reduction. Due to the fascinating electrochemical properties of POMs, the synthesis of new nanoparticle-POM hybrids would be expected to be promising candidates for the development of new type of electronic and optoelectronic devices. For example, facile transport of charge carries could be obtained compared to the case of the nanoparticles with organic capping ligands. Furthermore, nanoparticle-POM hybrids could also finely tune their surface plasmons via electrochemical reduction, which opens the door for the development of new sensors. Further studies for nanoparticle-POM hybrids along with detailed mechanistic investigations aiming to elucidate the products from the reduction process are underway.

EXPERIMENTAL SECTION

Synthesis.

$(TBA)_2[W_6O_{19}]$, $(TBA)_3[H_3V_{10}O_{28}]$, $(TBA)_4[H_4W_{12}O_{40}]$, $(TBA)_6[P_2W_{18}O_{62}]$, $(TBA)_{13}H_{23}K_4[P_2W_{48}O_{184}]$. The TBA salts of the POM clusters were synthesized according to previous reported literature.[44–46]

$(TBA)_5[HP_2W_{15}V_3O_{62}(C_{21}H_{19}N)]$. $(TBA)_5[H_4P_2V_3W_{15}O_{62}]$[47] (3.0g, 0.58 mmol) is dissolved in 30 ml of acetonitrile. Tris-pyrene[48] ($(HOCH_2)_3CNH\text{-}CH_2\text{-}C_{16}H_9$, 200 mg, 0.60 mmol) is added and the resulting solution is refluxed in the dark for 5 days. The solution is cooled down to room temperature before adding it dropwise to a large excess of diethyl ether with vigorous stirring to form a yellow precipitate. The precipitate is collected and re-dissolved in acetonitrile. Pure $(TBA)_5[HP_2W_{15}V_3O_{62}(C_{21}H_{19}N)]$ is obtained by re-precipitation in diethyl ether. Yield: (2.818 g, 0.52 mmol, 89 %); ^{1}H.NMR (400 MHz, CD_3CN): δ 9.20-7.10 (m, 8H), δ 5.93 (s, 2H), δ 5.64 ppm (s, 6H) in addition to the TBA resonances; Anal. Calcd for $C_{101}H_{200}N_6P_2W_{15}V_3O_{62}$ (5463.04 g mol^{-1}): C, 22.21; H, 3.69; N, 1.54; Found: C, 22.24; H, 3.89; N, 1.68.

$AuNO_3(PMe_3)$. $AuNO_3(PMe_3)$ was synthesized according to previous report.

Gold nanoparticle-POM hybrids. In a typical experiment, $AuNO_3(PMe_3)$ (7.7 mg, 25 μmol) and $(TBA)_4[H_4W_{12}O_{40}]$ (9.6 mg, 2.5 μmol) were dissolved in CH_3CN (20 ml) in Pyrex microwave vial and the sealed reaction mixture was then placed in microwave reactor and heated to 120 °C for 12 h. The resulting purple solution with gold nanoparticles gives a crude yield >50% in all cases. However, the crude material is contaminated with excess unreacted POMs. To purify the AuNP-POM hybrids, they were transferred into a dialysis membrane tube composed of cellulose (Molecular Weight Cut Off = 3500) and was dialyzed for 24 h using 1000 ml of the mixture containing CH_3CN and water (1:1, v/v) to remove unreacted $(TBA)_4[H_4W_{12}O_{40}]$ and this process was repeated two times. The use of dialysis membrane was essential to remove any aggregates of unreacted POM species which prevented the observation of the POM-NP hybrids as evidenced by TEM of the reaction mixture before the dialysis process. The yield after dialysis in all cases was in the 4-5% range. After dialysis treatment, the solution was concentrated bye ca. 10 times by evaporation of the relevant amount of solvent, followed by depositing the solution dropwise onto a carbon-coated TEM grid. The size distribution of gold nanoparticles was measured using calibrated TEM images by ImageJ software (a public domain image and analysis processing program).

Characterization. UV-Vis spectra were collected using JASCO V-670 spectrometer in absorbance mode using quartz cuvettes with 1.0 cm optical path length. Microwave-assisted reactions were performed using a CEM Discovery microwave. DLS measurements were recorded using a Malvern Instruments Zetasizer Nano ZS instrument at 25 °C. ^{31}P.NMR spectra were recorded on a Bruker DPX 400. All δ values are given in ppm. PXRD patterns were collected on a Philips X-pert diffractometer (λ(CuKα) = 1.5405 Å) equipped with PW3710 control unit. ESI-MS measurements were carried out at 30 °C using a Bruker micro ToF-Q in negative ion mode. TEM and EFTEM images were recorded on FEI Tecnai T20 transmission electron microscope equipped with Gatan Imaging Filter.

ASSOCIATED CONTENT

Supporting Information

The Supporting Information is available free of charge on the ACS Publications website at http://pubs.acs.org.

DLS, ESI-MS spectra, TEM images and TGA analysis (PDF).

AUTHOR INFORMATION

Corresponding Authors

* Prof. L. Cronin, Dr. H. N. Miras
E-mail:lee.cronin@glasgow.ac.uk;
Charalampos.moiras@Glasgow.ac.uk;

School of Chemistry, WestCHEM, University of Glasgow, Glasgow, G12 8QQ, U.K.

ORCID

Leroy Cronin: 0000-0001-8035-5757

Haralampos N. Miras: 0000-0002-0086-5173

Notes

The authors declare no competing financial interests.

ACKNOWLEDGEMENTS

We gratefully acknowledge financial support from the EPSRC for funding (grants EP/L023652/1, EP/R020914/1, EP/L023652/1, EP/R01308X/1, EP/K023004/1, EP/H024107/1, EP/I033459/1 and EP/J015156/1) the University of Glasgow, and the ERC (project 670467 SMART-POM) and LC thanks the Royal-Society Wolfson Foundation for a Merit Award. Y.-F S. thanks the National Key Research and Development Program of China (2017YFB0307303), the National Nature Science Foundation of China (NFSC), and Beijing Advanced Innovation Center for Soft Matter Science and Engineering (BAIC-SM) for financial support. We thank Donald A. MacLaren for EM measurements.

REFERENCES

(1) Pope, M. T.; Müller, A. Polyoxometalate Chemistry. *Angew. Chem. Int. Ed. Engl.* **1991**, *30*, 34–48.

(2) Miras, H. N.; Yan, J.; Long, D.-L.; Cronin, L. Engineering polyoxometalates with emergent properties. *Chem. Soc. Rev.* **2012**, *41* (22), 7403–7430.

(3) Long, D. L.; Tsunashima, R.; Cronin, L. Polyoxometalates: Building blocks for functional nanoscale systems. *Angew. Chem. Int. Ed.* **2010**, *49* (10), 1736–1758.

(4) Mizuno, N.; Misono, M. Heterogeneous Catalysis. *Chem. Rev.* **1998**, *98* (1), 199–218.

(5) Kozhevnikov, I. V. Catalysis by Heteropoly Acids and Multicomponent Polyoxometalates in Liquid-Phase Reactions. *Chem. Rev.* **1998**, *98* (1), 171–198.

(6) Rhule, J. T.; Hill, C. L.; Judd, D. A.; Schinazi, R. F. Polyoxometalates in Medicine. *Chem. Rev.* **1998**, *98* (1), 327–358.

(7) Yamase, T. Photo- and electrochromism of polyoxometalates and related materials. *Chem. Rev.* **1998**, *98* (1), 307–326.

(8) a) Keita, B.; Liu, T.; Nadjo, L. Synthesis of remarkably stabilized metal nanostructures using polyoxometalates. *J. Mater. Chem.* **2009**, *19* (1), 19–33; b) Zhang, M.; Hao, J.; Neyman, A.; Wang, Y.; Weinstock, I. A. *Inorg. Chem.* **2017**, *56*, 2400-2408.

(9) Wang, Y.; Weinstock, I. A. Polyoxometalate-decorated nanoparticles. *Chem. Soc. Rev.* **2012**, *41* (22), 7479.

(10) a) Zoladek, S.; Rutkowska, I. A.; Skorupska, K.; Palys, B.; Kulesza, P. J. Fabrication of polyoxometallate-modified gold nanoparticles and their utilization as supports for dispersed platinum in electrocatalysis. *Electrochim. Acta* **2011**, *56* (28), 10744–10750; b) Ozkar, S.; Finke, R. G. Nanoparticle Nucleation is Tetramolecular in Metal and Invvolves Hydrohgen: Evidence for a Kinetically Effective Nucleus of Three $\{Ir_3H_{2x}P_2W_{15}Nb_3O_{62}\}^{6-}$ in $Ir(0)_n$ Nanoparticle Formation From $[(1,5\text{-COD})Ir^{I}\ P_2W_{15}Nb_3O_{62}]^{8-}$ Plus Dihydrogen. *J. Am. Chem. Soc.*, **2017**, *139*, 5444-5457.

(11) a) Lin, Y.; Finke, R. G. Novel Polyoxoanion- and Bu_4N^+-Stabilized, Isolable, and Redissolvable, 20-30-.ANG. Ir300-900 Nanoclusters: The Kinetically Controlled Synthesis, Characterization, and Mechanism of Formation of Organic Solvent-Soluble, Reproducible Size, and Reproducible Catalytic Activity Metal Nanoclusters. *J. Am. Chem. Soc.* **1994**, *116* (18), 8335–8353; b) Lin, Y.; Finke, R. G. A More General Approach to Distingushing "Homogeneous" from "Heterogeneous" Catalysis: Discovery of Polyoxoanion- and BuN_4^+ Stabilized, Isolable and REdissolvable, High-Reactivity Ir.apprx. 190-450 Nanocluster Catalysts. *Inorg. Chem.* **1994**, *33*, 4891–4910.

(12) Aiken, J. D.; Finke, R. G. Nanocluster formation synthetic, kinetic, and mechanistic studies. The detection of, and the methods to avoid, hydrogen mass-transfer limitations in the synthesis of polyoxoanion- and tetrabutylammonium-stabilized, near- monodisperse 40 ± 6 Å Rh(0) nanoclusters. *J. Am. Chem. Soc.* **1998**, *120* (37), 9545–9554.

(13) Yuan, J. H.; Chen, Y. X.; Han, D. X.; Zhang, Y. J.; Shen, Y. F.; Wang, Z. J.; Niu, L. Synthesis of highly faceted multiply twinned gold nanocrystals stabilized by polyoxometalates. *Nanotechnology* **2006**, *17* (18), 4689–4694.

(14) Maayan, G.; Neumann, R. Direct aerobic epoxidation of alkenes catalyzed by metal nanoparticles stabilized by the $H_5PV_2Mo_{10}O_{40}$ polyoxometalate. *Chem. Commun.* **2005**, No. 36, 4595.

(15) Maayan, G.; Neumann, R. Direct aerobic oxidation of secondary alcohols catalysed by Pt(0) nanoparticles stabilized by $[PV_2Mo_{10}O_{40}]^{5-}$ polyoxmetalate. *Catal. Letters* **2008**, *123* (1–2), 41–45.

(16) Chalkley, L. The Extent of the Photochemical Reduction of Phosphotungstic Acid. *J. Phys. Chem.* **1952**, *56* (9), 1084–1086.

(17) Troupis, A.; Hiskia, A.; Papaconstantinou, E. *Angew. Chem. Int. Ed.* **2002**, *41*, 1911-1914.

(18) Troupis, A.; Gkika, E.; Hiskia, A.; Papaconstantinou, E. Photocatalytic reduction of metals using polyoxometallates: recovery of metals or synthesis of metal nanoparticles. *Compt. Rend. Chim.* **2006**, *9* (5–6), 851–857.

(19) Mandal, S.; Selvakannan, P. R.; Pasricha, R.; Sastry, M. Keggin ions as UV-switchable reducing agents in the synthesis of Au core-Ag shell nanoparticles. *J. Am. Chem. Soc.* **2003**, *125* (28), 8440–8441.

(20) Mandal, S.; Das, A.; Srivastava, R.; Sastry, M. Keggin ion mediated synthesis of hydrophobized Pd nanoparticles for multifunctional catalysis. *Langmuir* **2005**, *21* (6), 2408–2413.

(21) Gordeev, A. V; Kartashev, N. I.; Ershov, B. G. Metal Nanoparticles with $[PW_{11}O_{39}]^{7-}$ and $[P_2W_{17}O_{61}]^{10-}$ Heteropoly Anions as Stabilizing Agents: Radiation-Chemical Preparation and Properties. *High Energy Chem.* **2002**, *36* (2), 75–79.

(22) Zhang, G.; Keita, B.; Biboum, R. N.; Miserque, F.; Berthet, P.; Dolbecq, A.; Mialane, P.; Catala, L.; Nadjo, L. Synthesis of various crystalline gold nanostructures in water: The polyoxometalate β-$[H_4PMo_{12}O_{40}]^{3-}$ as the reducing and stabilizing agent. *J. Mater. Chem.* **2009**, *19* (45), 8639.

(23) Hsu-Yao, T.; Browne, K. P.; Honesty, N.; Tong, Y. J. Polyoxometalate-stabilized Pt nanoparticles and their electrocatalytic activities. *Phys. Chem. Chem. Phys.* **2011**, *13* (16), 7433.

(24) Zhang, G.; Keita, B.; Dolbecq, A.; Mialane, P.; Sécheresse, F.; Miserque, F.; Nadjo, L. Green Chemistry-Type One-Step Synthesis of Silver Nanostructures Based on Mo. *Chem. Mater.*, **2007**, *19*, 5821–5823.

(25) Keita, B.; Zhang, G.; Dolbecq, A.; Mialane, P.; Se, F.; Nadjo, L. Mo V -Mo VI Mixed Valence Polyoxometalates for Facile Synthesis of Stabilized Metal Nanoparticles : Electrocatalytic Oxidation of Alcohols. *J. Phys. Chem. C*, **2007**, *4* (1), 8145–8148.

(26) Liu, R.; Li, S.; Yu, X.; Zhang, G.; Zhang, S.; Yao, J.; Keita, B.; Nadjo, L.; Zhi, L. Facile synthesis of Au-nanoparticle/polyoxometalate/graphene tricomponent nanohybrids: An enzyme-free electrochemical biosensor for hydrogen peroxide. *Small* **2012**, *8* (9), 1398–1406.

(27) Lica, G. C.; Browne, K. P.; Tong, Y. *J.* Interactions between Keggin-type lacunary polyoxometalates and ag nanoparticles: A surface-enhanced raman scattering spectroscopic investigation. *Clust. Sci.* **2006**, *17* (2), 349–359.

(28) Ernst, A. Z.; Sun, L.; Wiaderek, K.; Kolary, A.; Zoladek, S.; Kulesza, P. J.; Cox, J. A. Synthesis of polyoxometalate-protected gold nanoparticles by a ligand-exchange method: Application to the electrocatalytic reduction of bromate. *Electroanalysis* **2007**, *19* (19–20), 2103–2109.

(29) Neyman, A.; Meshi, L.; Zeiri, L.; Weinstock, I. A. Direct imaging of the ligand monolayer on an anion-protected metal nanoparticle through cryogenic trapping of its solution-state

structure. *J. Am. Chem. Soc.* **2008**, *130* (49), 16480–16481.
(30) Wang, Y.; Neyman, A.; Arkhangelsky, E.; Gitis, V.; Meshi, L.; Weinstock, I. A. Self-assembly and structure of directly imaged inorganic-anion monolayers on a gold nanoparticle. *J. Am. Chem. Soc.* **2009**, *131* (47), 17412–17422.
(31) Wang, Y.; Zeiri, O.; Sharet, S.; Weinstock, I. A. Role of the alkali-metal cation size in the self-assembly of polyoxometalate-monolayer shells on gold nanoparticles. *Inorg. Chem.* **2012**, *51* (14), 7436–7438.
(32) Colton, R.; D'Agostino, A.; Traeger, J. C. Electrospray mass spectrometry applied to inorganic and organometallic chemistry. *Mass Spectrom. Rev.* **1995**, *14* (2), 79–106.
(33) Henderson, W.; Nicholson, B. K.; McCaffrey, L. J. Applications of electrospray mass spectrometry in organometallic chemistry. *Polyhedron* **1998**, *17*, 4291–4313.
(34) Johnson, B. F. G.; McIndoe, J. S. Spectroscopic and mass spectrometric method for the characterisation of metal clusters. *Coord. Chem. Rev.* **2000**, *200–202*, 901–932.
(35) Yuan, Y.; Kozlova, A. P.; Asakura, K.; Wan, H.; Tsai, K.; Iwasawa, Y. Supported Au Catalysts Prepared from Au Phosphine Complexes and As-Precipitated Metal Hydroxides: Characterization and Low-Temperature CO Oxidation. *J. Catal.* **1997**, *170* (1), 191–199.
(36) Miras, H. N.; Wilson, E. F.; Cronin, L. Unravelling the complexities of inorganic and supramolecular self-assembly in solution with electrospray and cryospray mass spectrometry. *Chem. Commun.* **2009**, No. 11, 1297–1311.
(37) Miras, H. N.; Long, D.-L.; Kögerler, P.; Cronin, L. Bridging the gap between solution and solid state studies in polyoxometalate chemistry: discovery of a family of $[VM_{17}]$-based cages encapsulating two $\{V^{V}O_4\}$ moieties. *Dalton Trans.* **2008**, 214–221.
(38) Wilson, E. F.; Miras, H. N.; Rosnes, M. H.; Cronin, L. Real-time observation of the self-assembly of hybrid polyoxometalates using mass spectrometry. *Angew. Chem. Int. Ed.* **2011**, *50* (16), 3720–3724.
(39) Jun Yan; De-Liang Long; Haralampos, N. M.; Cronin, L. Cation controlled assembly and transformation of mono-and Bi-sulfite templated dawson-type polyoxotungstates. *Inorg. Chem.* **2010**, *49* (4), 1819–1825.
(40) Xu, F.; Scullion, R. A.; Yan, J.; Miras, H. N.; Busche, C.; Scandurra, A.; Pignataro, B.; Long, D. L.; Cronin, L. A supramolecular heteropolyoxopalladate {Pd15} cluster host encapsulating a {Pd2} dinuclear guest: $[Pd^{II}_2\{H_7Pd^{II}_{15}O_{10}(PO_4)_{10}\}]^{9-}$. *J. Am. Chem. Soc.* **2011**, *133* (13), 4684–4686.
(41) Eustis, S.; El-Sayed, M. A. Molecular mechanism of the photochemical generation of gold nanoparticles in ethylene glycol: Support for the disproportionation mechanism. *J. Phys. Chem. B* **2006**, *110* (29), 14014–14019.
(42) Bergamini, G.; Ceroni, P.; Balzani, V.; Gingras, M.; Raimundo, J.-M.; Morandi, V.; Merli, P. G. Synthesis of small gold nanoparticles: Au(I) disproportionation catalyzed by a persulfurated coronene dendrimer. *Chem. Commun. (Camb).* **2007**, *1* (40), 4167–4169.
(43) Das, A. K.; Raj, C. R. Iodide-mediated reduction of AuCl4- and a new green route for the synthesis of single crystalline Au nanostructures with pronounced electrocatalytic activity. *J. Phys. Chem. C* **2011**, *115* (43), 21041–21046.
(44) Himeno, S.; Yoshihara, M.; Maekawa, M. Formation of voltammetrically-active isopolyoxotungstate complexes in aqueous CH_3CN media. *Inorg. Chim. Acta* **2000**, *298* (2), 165–171.
(45) McGlone, T.; Thiel, J.; Streb, C.; Long, D.-L.; Cronin, L. An unprecedented silver-decavanadate dimer investigated using ion-mobility mass spectrometry. *Chem. Commun.* **2012**, *48* (3), 359–361.
(46) Gabb, D.; Pradeep, C. P.; Boyd, T.; Mitchell, S. G.; Miras, H. N.; Long, D. L.; Cronin, L. A general route for the transfer of large, highly-charged polyoxometalates from aqueous to organic phase. *Polyhedron* **2013**, *52*, 159–164.
(47) Finke, R. G.; Rapko, B.; Saxton, R. J.; Domaille, P. J. Trisubstituted heteropolytungstates as soluble metal oxide analogs. III. Synthesis, characterization, phosphorus-31, silicon-29, vanadium-51, and 1- and 2-D tungsten-183 NMR, deprotonation, and proton mobility studies of organic solvent solute forms of $[H_xSiW_9V_3O_{40}]^{x-7}$ and $[H_xP_2W_{15}V_3O_{62}]^{x-9}$. *J. Am. Chem. Soc.* **1986**, *108* (11), 2947–2960.
(48) Song, Y. F.; Long, D. L.; Cronin, L. Noncovalently connected frameworks with nanoscale channels assembled from a tethered polyoxometalate-pyrene hybrid. *Angew. Chem. Int. Ed.* **2007**, *46* (21), 3900–3904.